RSC Advances

ROYAL SOCIETY OF CHEMISTRY

PAPER

View Article Online
View Journal | View Issue

Check for updates

Cite this: *RSC Adv.*, 2020, **10**, 40806

Probing the high performance of photoinduced birefringence in V-shaped azo/PMMA guest–host films†

Lidiana M. Silva,[a] Daniel L. Silva,[b] Mariana V. Boas,[a] Yann Bretonniere,[c] Chantal Andraud[c] and Marcelo G. Vivas *[a]

Received 30th September 2020
Accepted 29th October 2020

DOI: 10.1039/d0ra08379h

rsc.li/rsc-advances

Optical birefringence in polymeric films containing azo-chromophores is an important feature related to the development of several technologies such as electro-optic modulators, optical switching, and optical gates, to cite a few. Therefore, it is essential to understand the main underlying mechanisms describing dynamic switching. In this context, we have investigated the optical birefringence performance of a guest–host film produced from a poly(methyl methacrylate) (PMMA) matrix containing a V-shaped azo-chromophore, which exhibited a larger optical response in comparison to the linear chromophores. The optical birefringence was induced by a linearly polarized diode laser (532 nm, writing laser), while a low-intensity HeNe (632.8 nm) laser and a tungsten-halogen lamp are employed, respectively, to monitor the optical storage and the absorption change during the photoinduced birefringence. Our results pointed out that the guest–host film presents maximum residual optical memory at around 50% and local optical birefringence at around 3.3×10^{-4} in the low concentration and intensity regimes. The high optical birefringence obtained in guest–host films was attributed to the considerable photoisomerization quantum yield in the solid-state (0.15 ± 0.02 for 532 nm). Besides, we have shown that the switching mechanism is driven by angular hole-burning during the first seconds after excitation, and, subsequently, molecular reorientation quickly rises, dominating the photochemical process. The latter mechanism is highly efficient in converting *cis* to *trans* molecules (100%), which is responsible for the high residual optical memory obtained. In order to better understand the isomerization mechanism of the azo-chromophore/PMMA film, we performed quantum chemical calculations within the DFT framework. The electronic transitions of the azo-chromophore isomers were determined using the TD-DFT method and potential energy curves (PECs) were constructed to investigate the possibility of the thermal-isomerization process of the V-shaped azo-chromophore through both rotation and inversion mechanisms. For both mechanisms, the amplitude of the energy barrier and activation energy for thermal isomerization are determined and the results are discussed.

1. Introduction

Due to their ultrafast and efficient photoisomerization process, azo-chromophores have been widely studied for the development of several photonic devices such as surface-relief gratings, nanodevices for electro-optical modulators, all-optical switching, micro-resonators, logic gates, 3D optical storage and so on.[1–20] Moreover, azo-chromophores have presented high nonlinear optical responses such as two-photon absorption, second harmonic generation, and first-order hyperpolarizability.[21–24]

Azoaromatic compounds can be found in two configurations, *trans* and *cis* isomers, in which the *cis* is more unstable due to closer aromatic rings, causing a stronger electronic repulsion. The switching mechanism (*trans*–*cis* and *cis*–*trans*) can be triggered by light from UV-visible to near-infrared region, and it is called photoisomerization. This photochemical process plays a central role in the photoinduced optical birefringence in polymers containing azo-chromophores. According to ref. 25, such a goal is achieved due to two main mechanisms. The first one is called the angular hole burning (AHB), in which the light isomerizes chromophores initially in the *trans* configuration, having an electric dipole moment component projected on the light polarization. Subsequently, there is relaxation from *cis* to *trans* configuration caused by molecular

---

[a] *Laboratório de Espectroscopia Óptica e Fotônica, Universidade Federal de Alfenas, Poços de Caldas, MG, Brazil. E-mail: mavivas82@gmail.com*

[b] *Departamento de Ciências da Natureza, Matemática e Educação, Universidade Federal de São Carlos, Rod. Anhanguera – Km 174, 13600-970 Araras, SP, Brazil*

[c] *Univ. Lyon, ENS de Lyon, CNRS UMR 5182, Université Claude Bernard Lyon 1, Laboratoire de Chimie, F69342, Lyon, France*

† Electronic supplementary information (ESI) available. See DOI: 10.1039/d0ra08379h

reorientation (MRO),[25] and when there is no excitation arises randomly. Thus, combining these two mechanisms, for a linearly polarized excitation, a set of several *trans–cis–trans* cycles tends to align the chromophores perpendicularly to the light polarization because they are no longer isomerized by the excitation beam.

In general, to obtain an efficient device based on optical switching in azo-chromophores, four different parameters are essential: (i) high electronic transition rate (related to the molar absorptivity), (ii) high photoisomerization quantum yield, (iii) a steady-state relative abundance of *trans* and *cis* isomers at room temperature and (iv) the reproducibility of photochemical switching over time.[1,26,27] Hence, these parameters need to be available.

In the last decades, the linear azo-chromophore dyes such as the disperse red (DR) family have been widely studied for optical storage applications. However, this class of organic molecules presents low optical birefringence and residual optical memory due to the small photoisomerization quantum yield and optical absorption.[28–30] Otherwise, azo-chromophores with branched structures such as V-shaped, Y-shaped, and multi-branched (dendrimers) have emerged as an alternative synthesis route to tune and enhance the optical response of organic materials.[31,32] For example, ref. 33 and 34 have shown that the V-shaped molecules may present higher linear and nonlinear optical responses than linear molecules. In this context, we have investigated optical storage performance based on photoinduced birefringence of guest–host films containing V-shaped azo-chromophores in the poly(methyl methacrylate) (PMMA) matrix. The molecular structure of the V-shaped azo-chromophore is illustrated in Fig. 1(a).

This study aims to understand the underlying mechanism that rules the high performance of optical birefringence obtained in this present work. For that, we have performed several experiments in which we observed the formation and relaxation times and residual optical memory for optical birefringence as a function of the power laser. The ground-state transient absorption also was monitored to aid understanding of the photoisomerization process. These results were explained based on the photoisomerization quantum yield and the AHB and MRO contributions obtained for the switching mechanism based on the Kawabe *et al.*[29] approach. Moreover, we have studied the nature of the isomerization mechanism for the V-shaped azo-chromophore by employing quantum chemical calculations.

2. Experimental

We have studied two films with different dye concentrations. The films were prepared from a mixture of PMMA/chloroform solution (160 mg ml^{-1}) with a solution of 2.0 mg ml^{-1} (1.25 w/w%, Film 1) or 0.09 mg ml^{-1} (0.056 w/w%, Film 2, see Fig. 1(b)) of azo-chromophore/chloroform. The azo-chromophore/PMMA solution (400 µl) was cast onto a circular glass substrate (diameter of 2.54 cm). The glass substrate was placed on a Petri plate and left in a chloroform-rich environment. The films were left to dry slowly at room temperature for 6 hours. Details about the synthesis of the azo-chromophore can be found in ref. 32. The PMMA (average $M_w \sim 120.000$, $T_g = 105\ ^\circ C$ (midpoint)) was purchased from Sigma-Aldrich. The film thickness was measured from optical microscopy, according to ref. 35, and values 120 ± 15 µm were found.

The first experiment performed was to measure the induced optical birefringence. In this experiment, the optical birefringence is induced by a cw diode laser (writing laser) at 532 nm with vertical polarization (0.2–10 mW). For the reading laser, we employed a low-intensity HeNe laser (<0.1 mW, at 632.8 nm) with a polarization angle of 45° with respect to the polarization of the writing beam. The reading laser passes through the sample, and by a crossed polarizer (−45°) positioned after the sample that acts as an analyzer. The writing laser induces birefringence such that a fraction of the reading laser beam passes through the analyzer, and it is detected by the silicon photodetector. Thus, the reading laser transmittance is used to

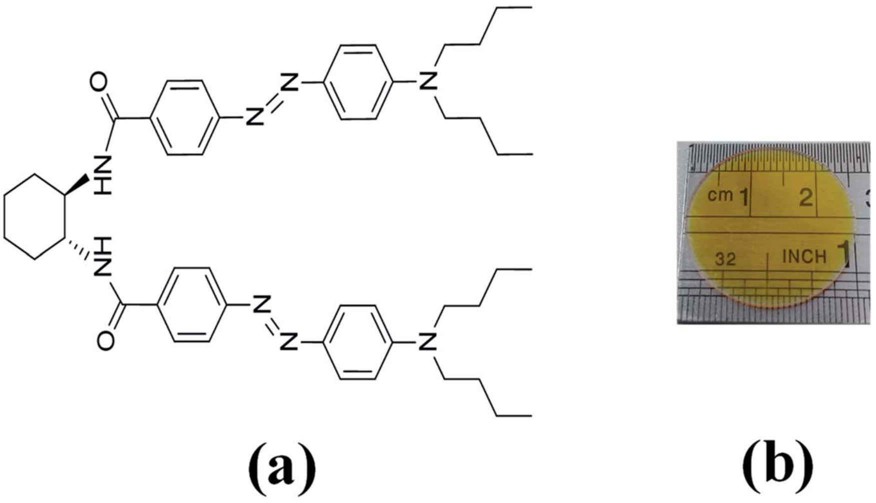

Fig. 1 (a) Molecular structure of V-shaped azo-chromophore. (b) V-shape azo-chromophore/PMMA guest–host film.

monitor photoinduced birefringence over time, which requires a precise superposition of both beams in the sample. The diameter of the reading (green laser and white-light) and writing (HeNe) laser were of 2 mm and 3 mm, respectively, which were measured through the knife-edge technique. In the second experiment, we have changed the reading laser by a stabilized tungsten-halogen lamp and the photodetector by an optical fiber coupled to the spectrometer to measure in real-time the absorption change during the photoinduced birefringence. Such a procedure was performed for the white-light with parallel and perpendicular polarization with respect to the writing laser. In both experiments, we have used a shutter to switch on and off the writing laser. The experiments were automatically controlled by dedicated software. In all measurements, the wait time for the formation and relaxation of the optical birefringence was of 200 s and 100 s, respectively.

3. Theoretical calculations

Quantum chemical (QC) calculations were performed using Gaussian 09 package.[36] All QC calculations were conducted at the density functional theory (DFT) level[37,38] using the hybrid B3LYP functional[39,40] and the 6-31G(d,p) basis set for H and C atoms and 6-31+G(d,p) basis set for N and O atoms. The geometry optimization calculations were performed with the molecule isolated (gas-phase) and in the $CHCl_3$ solvent. In the solvated case, the self-consistent reaction field (SCRF) method based on the polarizable continuum model using the integral equation formalism variant (IEF-PCM),[41] as implemented in Gaussian 09 package, was employed. The geometry optimization calculations were performed free of constraints.

We also have calculated the ground-state potential energy curves (PEC) starting from either the *trans* or *cis* optimized geometry to investigate the thermal isomerization process of V-shaped azo-chromophore. By constraining the C–N═N–C dihedral angle or one of the C–N═N bond angles, while optimizing all the other structural parameters, the rotation and inversion mechanisms of the isomerization were respectively investigated. The constrained angle was incremented in 10° steps, between the *cis* and *trans* isomer structures, and the energy of the optimized structure with zero-point energy corrections obtained at each point.

The energy barrier of the thermal *trans–cis* isomerization process was computed as the difference between the DFT energies with zero-point energy corrections of the *trans* isomer and the one of the transition state (TS). Moreover, the activation energy (E_a) of the kinetics of the thermal *cis–trans* isomerization was computed as the difference between the DFT energies with zero-point energy corrections of the *cis* isomer and the one of the transition state (TS). The nature of the two isomers stationary points and the transition state were confirmed by vibrational frequency analysis.

Time-Dependent Density Functional Theory (TD-DFT)[42] was employed for computing the UV/vis spectra of the V-shaped azo-chromophore in gas-phase and $CHCl_3$ solvent. Indeed, TD-DFT is often found robust and efficient for evaluating the low-lying excited spectra of organic and inorganic conjugated molecules and has been the subject of numerous applications aiming at providing a rationalization of experimental absorption spectra. In addition, the most appealing characteristic of TD-DFT is its ability to produce at a relatively small computational cost accurate electronic transition energies and intensities. The ten singlet lowest-energy of the two isomers of V-shaped azo-chromophore were determined and using the eight lowest-energy ones their absorption spectrum was simulated by the superposition of individual Lorentzian lines with a full width at half-maximum (FWHM) of 0.40 eV.

4. Results and discussions

The ground-state absorption spectrum for the V-shaped azo-chromophores/PMMA in solution (solid line) and film (dashed line) is shown in Fig. 2(a). As noted, for both solution and film forms, the azo-chromophore presents a wide absorption band located at 448 nm, which is related to the π–π* transition. It is also observed that the film is completely transparent for the reading laser wavelength (632.8 nm). Details about the electronic and optical features for this molecule can be found in ref. 32.

In Fig. 2(b), we illustrated the results obtained for the calculations of the absorption cross-section (or molar

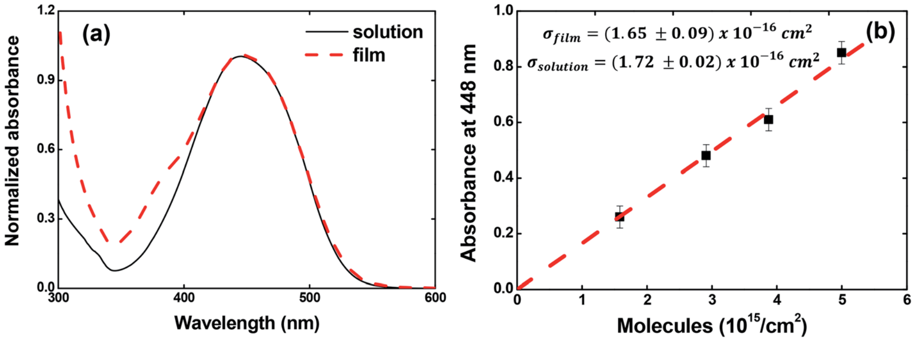

Fig. 2 (a) Absorption spectrum for V-shaped azo-chromophores/PMMA in chloroform solution (solid line) and guest–host film (dash line). (b) Absorbance at 448 nm as a function of the concentration.

absorptivity) for the guest–host films, which is very important to calculate the photoisomerization quantum yield. For that, we measured the absorption spectrum for four films containing different concentrations of azo-chromophores. The absorption spectrum for the films containing different chromophores concentrations can be found in Fig. SI.1 (see ESI).† Our results pointed out that the absorption cross-section value to the film is the same observed in solution within the experimental error (σ_{film} (448 nm) = $(1.65 \pm 0.09) \times 10^{-16}$ cm^2 and σ_{solution} (448 nm) = $(1.72 \pm 0.02) \times 10^{-16}$ cm^2 or equivalently ε (448 nm) = 4.31×10^4 M^{-1} cm^{-1}). These results confirm the high optical quality of the guest–host films.

In solid-state, the V-shaped azo-chromophore exhibits a shoulder at 380 nm as compared to the solution. In order to gain a deeper understanding of the azo-chromophore/PMMA film optical features, we have performed quantum chemical calculations within the DFT framework. The simulated absorption spectrum of the V-shaped molecule in gas-phase and $CHCl_3$ is presented in Fig. 3(a). It is worth mentioning that the implicit solvation PCM, as implemented in the Gaussian package, adopts a dielectric constant (or refractive index) for chloroform solvent very similar to the one of the PMMA matrix. Moreover, the absorption spectrum of a reduced version of V-shaped azo-chromophore was also simulated. Such a reduced version was obtained by substituting the four saturated chains of the molecules to ethyl groups. Since the main role of such chains is to increase the solubility of the molecule, being in principle secondary their contribution for the V-shaped electronic structure, it was expected that the effects of such substitutions on the absorption spectrum would be small. The simulated absorption spectra of the reduced V-shaped azo-chromophore molecule in gas-phase and $CHCl_3$ are presented in Fig. 3(b) and, as it was expected, the effects of the substitutions on the absorption spectrum were confirmed to be small.

From Fig. 3, it is observed that the simulated absorption spectrum of *trans*-isomer presents a single peak, centered at 460 nm. This feature is in agreement with the experimental absorption spectrum of *trans*-isomer, in which the absorption band peak is located at 448 nm. However, the results of the TD-DFT/PCM calculations point out that such absorption band should be ascribed to two electronic transitions of similar intensities ($f = 1.381$ and $f = 1.384$), separated by only 0.07 eV in energy, and both described by the HOMO−1 → LUMO and HOMO → LUMO+1 excitations. It is also observed that the simulated absorption spectrum of *trans*-isomer has a tail that extends to the red region (up to 600 nm). Such a feature is not observed in the experimental spectrum of the molecule in solution, which after 560 nm no longer shows any absorption. Such divergence from the theoretical description in relation to experimental observation may be related to the choice adopted in this work, for the sake of simplicity, of adopting a single Lorentzian linewidth value (0.40 eV) for all electronic transitions taken into consideration to simulate the spectrum.

As can be observed in Fig. 3, the absorption spectrum of *cis*-isomer presents two peaks, lowest-energy one located at 500 nm and the higher-energy one around 360–380 nm. In $CHCl_3$ solvent, the higher-energy peak of both the isomers and its reduced version is localized at 380 nm. Such observation sheds light on the issue of the shoulder observed in the absorption spectrum of the molecule in solid-state and confirms that such a shoulder should be ascribed to the contribution of the *cis*-isomer for the final absorption spectrum of the molecule in solid-state. The experimental absorption spectrum of V-shaped azo-chromophore in solution also shows some absorption in the region energetically above 350 nm (ultraviolet region). However, because only the eight lowest-energy transitions of the isomers were taken into account to simulate the absorption spectrum, such experimental information is not reproduced by the simulated spectra here presented.

As it is well-known, the isomerization process of azobenzene chromophores in rigid media depends strongly on the local environment and free volume distribution around the chromophores.[43–45] Thus, the appearance of a more significant contribution of the *cis*-isomers to the absorption in solid-state could, in principle, be understood in this way. Since a shoulder in the film absorption spectrum is observed just after the casting procedure onto a glass substrate, *i.e.*, before the film to be irradiated with laser light, the possibility of the isomerization process having a thermal origin was theoretically investigated. Potential energy curves (PECs) were constructed starting from either the *trans* or *cis* optimized geometry to investigate the possibility of the thermal-isomerization process

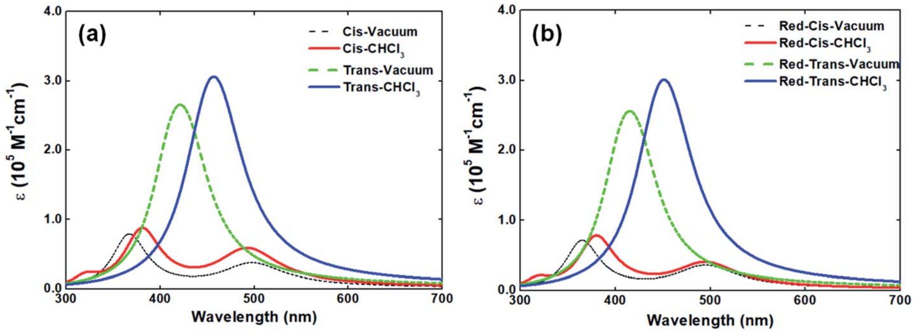

Fig. 3 Simulated absorption spectra of V-shaped azo-chromophore isomers (a) and their reduced version (b) in gas-phase and in $CHCl_3$ solvent. The spectra were simulated using the information provided by TD-DFT and TD-DFT/PCM calculations for the eight lowest-energy transitions and by the superposition of individual Lorentzian lines (FWHM = 0.40 eV).

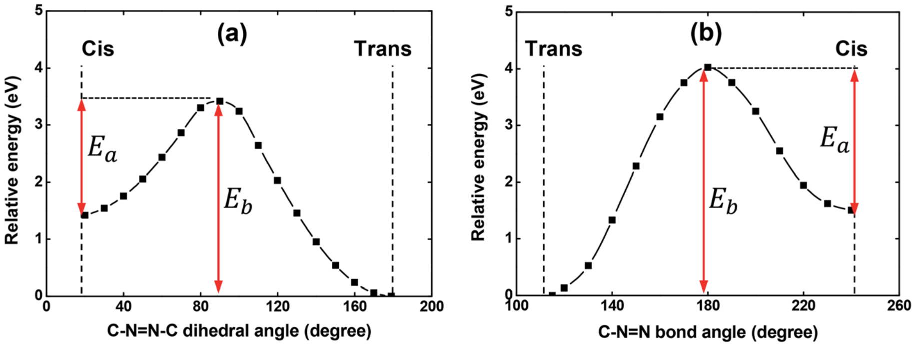

Fig. 4 The computed potential energy curve for thermal isomerization of V-shaped azo-chromophore molecule in gas-phase through the rotation (a) and inversion (b) mechanisms. The computed geometries of the *cis* and *trans* isomers and the transition state are also shown. E_b indicates the energy barrier of the thermal *trans*–*cis* isomerization and E_a indicates the activation energy of the kinetics of the thermal *cis*–*trans* isomerization.

through both the rotation and inversion mechanisms. These computations were performed with the V-shaped molecule in gas-phase.

The PECs obtained for the rotation and inversion mechanisms are shown in Fig. 4(a) and (b), respectively. For both mechanisms, the amplitude of the energy barrier (E_b) of the thermal *trans–cis* isomerization and the activation energy (E_a) for the thermal *cis–trans* isomerization are illustrated in Fig. 4. As can be observed, $E_b = 3.42$ eV (362 nm) and $E_b = 4.02$ eV (308 nm) for the mechanism of the rotation and inversion, respectively. For such high energies, the thermal contribution for the isomerization process of the V-shaped azo-chromophore can be basically discarded. Therefore, we are led to conclude that the observed isomerization process is photo-induced by the laboratory ambient light.

Concerning the activation energy of the thermal *cis–trans* isomerization kinetics, the values $E_a = 2.00$ eV and $E_a = 2.50$ eV were obtained for the mechanism of the rotation and inversion, respectively. Such values indicated that from the energetic point of view, the thermal *cis–trans* isomerization process would happen more easily through the rotation mechanism. However, some studies on the literature evidence that the rotation mechanism requires more space (free volume) to isomerize, while the inversion mechanism takes up less space when transitioning between the isomers.[43,46] Thus, for the results obtained here, a difference of only 0.50 eV between the activation energies, we believe that structural restrictions imposed by the polymeric matrix significantly hinder the isomerization process from evolving through the rotational pathway and, therefore, it is not possible to point out a predominant mechanism in the thermal *cis–trans* isomerization kinetics. Since the photoisomerization pathways were elucidated, we have performed photoinduced birefringence measurements.

Fig. 5 depicts the optical birefringence curves as a function of the laser power for Film 1 (Fig. 5(a)) and Film 2 (Fig. 5(b)). To calculate the photoinduced optical birefringence, we have used the following equation (valid for thick sample):

$$\Delta n = \frac{\lambda}{\pi L} \arcsin\left(\frac{P}{P_0}\right), \tag{1}$$

in which L is the film thickness, λ is the wavelength of the reading laser (632.8 nm), P and P_0 are laser power transmitted and incident of the reading laser, respectively. The first aspect to highlight in Fig. 5 is that Film 1 presents higher Δn and residual optical memory (fraction of optical birefringence at 320 s) values due to their higher density of chromophores. At the same time, Δn values as high as 3.0×10^{-4} (for guest–host films) were obtained for a laser power above 2 mW. The second one highlights the large residual optical memory obtained, between 30% and 50% (compared to the maximum optical birefringence), depending on the laser power. For example, residual optical memories obtained for the DR family in

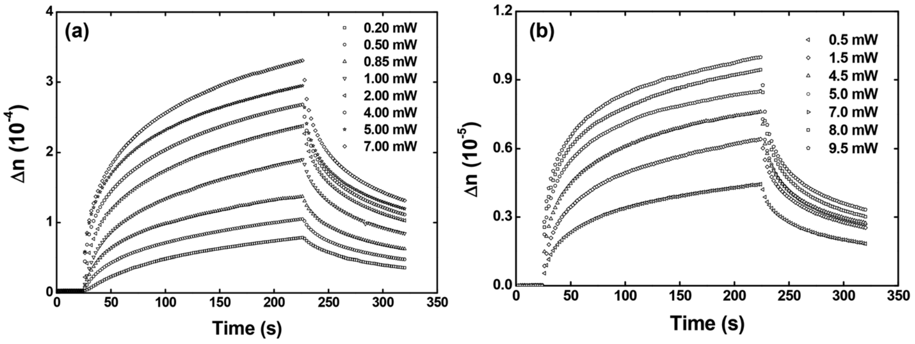

Fig. 5 Optical birefringence curves as a function of the writing laser power for the (a) Film 1 and (b) Film 2.

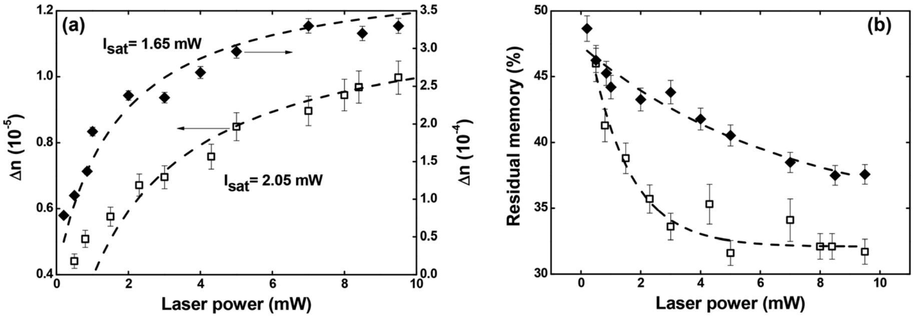

Fig. 6 (a) Maximum optical birefringence and (b) residual memory as a function of the writing laser power. Full diamonds and empty squares correspond, respectively, to Film 1 and Film 2.

a polymeric matrix are between 5% and 10%, and the optical birefringence signal is smaller than 1×10^{-4} for the samples with a low concentration (~1 w/w%).[28,47,48] Even when we compared the V-shaped molecule results with those found for chromophores of similar molecular geometry and experimental condition (thickness and chromophores concentration),[4] our outcomes are more promising, in particular, ones related to the residual optical memories. It is worth mentioning that such values need to be compared with the results found for guest–host films. To emphasize these important outcomes, in Fig. 6, we show the maximum optical birefringence (Fig. 6(a)) and residual memory (Fig. 6(b)) as a function of the writing laser power. From the fitting of Fig. 6(a) data, we can obtain the saturation power for Film 1 and Film 2 through the equation $\Delta n(P) \propto P/(P + P_{sat})$, in which P and P_{sat} are the writing and saturation power. The saturation power found was 1.65 mW for Film 1 (full diamonds) and 2.05 mW for Film 2 (empty squares). Therefore, a high optical birefringence ($\sim 3 \times 10^{-4}$) is achieved, even under low excitation power (<2 mW).

Regarding the residual optical memory (Fig. 6(b)), we have observed a similar behavior, *i.e.*, Film 1 presents a higher performance. Besides, a residual optical memory decrease is noticed as the laser power increase. It happens because of the higher laser power to generate larger thermal agitation, which increases the angular diffusion effect that tends to restore the isotropic thermodynamic equilibrium.[25] It is important to emphasize that in guest–host films, the chromophores are not covalently bonded to the polymer, and, therefore, there is great freedom for angular diffusion. In such a system, the van der Waals forces are predominantly responsible for the interaction between the chromophores and the host matrix.[49]

Concerning the temporal evolution of the optical birefringence mechanism, we have employed the bi-exponential model to obtain the formation and relaxation times.[50] Our results show that the slow (τ_1 and τ_3) and fast (τ_2 and τ_4) characteristic times for the formation and relaxation optical birefringence decrease as a function of the laser power (see Fig. SI.2 of the ESI†). Such behavior is characteristic of optical storage in guest–host films.[51] Moreover, all the times found are higher for Film 1 due to the higher chromophores density, which decreases the free volume to occur *trans* → *cis* → *trans* photoisomerization cycle (details on the formation and relaxation times can be found in ESI†).

To shed more light on the photoinduced birefringence mechanism, we have analyzed the absorption change for the guest–host films during the formation of optical birefringence. For this study, we have measured the absorption change only for Film 2, because Film 1 presents a very high absorption. This experiment was performed in two configurations using the white light with parallel and perpendicular polarization to the writing laser. Fig. 7(a) shows the absorption change at 448 nm (related to the peak of π–π* transition) as a function of the time

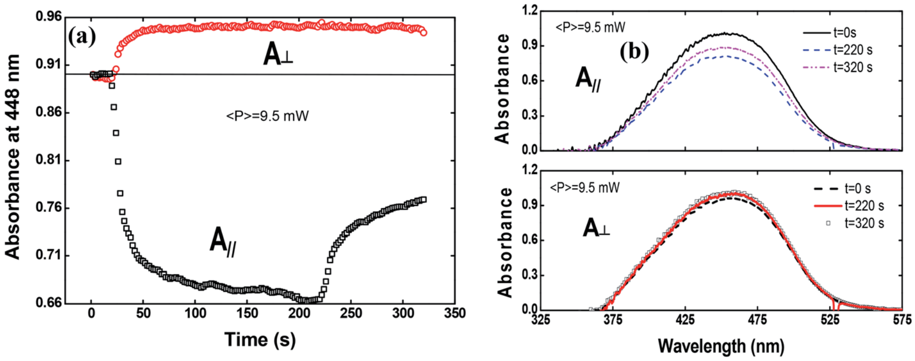

Fig. 7 (a) Absorption change at 448 nm (peak of absorption spectrum) as a function of the time for the perpendicular polarized (circles) and parallel (squares) light to the writing laser. (b) The absorption spectra for the three different times (initial, after turning off the writing laser and at the end of the experiment).

for the perpendicular (circles) and parallel (squares) polarization in respect to the writing laser.

The absorption spectra for the three different times along the temporal window of the experiment (at the first reading, when the writing laser is switched off and at the last reading) are illustrated in Fig. 7(b). For the white light polarization parallel to the writing laser, we observed a great reduction in the absorption during the first 15 seconds after the excitation. This behavior can be explained by the increase of chromophores aligned perpendicularly to the excitation laser, and, consequently, to the white light polarization, decreasing its absorption. After switching off the writing laser, the absorbance increase by only 45%. On the other hand, when the white light is perpendicularly polarized to the writing laser, the absorbance increases quickly and maintain such value during all time even after removing the excitation. Now, due to the AHB and MRO mechanisms, we have the polarization of white light in the same direction of the chromophores alignment. Thus, the projection of the radiation electric field is maximum on the dipole moment of the chromophores and, therefore, we observed an increase in the absorption. These two interesting outcomes suggested that the main photoinduced birefringence mechanism is related to the molecular reorientation. The absorption change for perpendicularly polarized white light is 1/3 compared to the parallel polarization. Therefore, we observed that, at the end of the experiment (t = 320 s), the average absorption ($\bar{A} = (A_{\parallel}(t) + 2A_{\perp}(t))/3$, as defined in ref. 25) to the π–π* transition returns to the initial value (A_i = 0.89), indicating that there was a complete conversion of the *cis* to *trans* isomers, corroborating the high contribution of the MRO mechanism. To stress such a result, in Fig. 8, we show the ground-state transient absorption spectra for the (Fig. 8(a)) perpendicular and (Fig. 8(b)) parallel polarization and (Fig. 8(c)) average absorption. As can be seen in Fig. 8, the behavior previously mentioned happens for all wavelengths (380–530 nm). Thus, we can conclude that, indeed, the MRO mechanism is responsible for returning the *cis* to *trans* molecules with 100% efficiency.

Recently, Kawabe *et al.*[29] have formulated a simple model to discriminate the contributions of the AHB due to photoisomerization and MRO on the optical switching mechanism for DR1 in PMMA. According to that model, the contributions of the AHB and MRO mechanism can be evaluated as:

$$\Delta A_{\mathrm{AHB}}(t) = -\frac{3}{5}\left(\Delta A_{\parallel}(t) + 2\Delta A_{\perp}(t)\right) \tag{2}$$

$$\Delta A_{\mathrm{MRO}}(t) = \frac{2}{5}\left(3\Delta A_{\perp}(t) - \Delta A_{\parallel}(t)\right) \tag{3}$$

in which ΔA indicates the absorption change, *i.e.*, $\Delta A(t) = A(t) - A(t=0)$. Fig. 9 shows the results obtained by employing the eqn (2) and (3).

As noted, after switching on the writing laser during the first seconds, the AHB dominates the process. However, after that, a quick rise of MRO mechanism achieved values 250% higher than the AHB for 9.5 mW. Similar behavior also was observed for lower laser power. When the results are compared to ones published in ref. 50 for PMMA/DR1, we observed that the dominant mechanism for the chromophores DR1 and V-shaped (this work) is distinct. For instance, we found the MRO, while the AHB was the dominant mechanism observed by them. This can explain the great difference obtained for residual optical memory as we compared the V-shaped molecule with the DR family.

We have also calculated the quantum yield of photoisomerization (*trans*–*cis*) for the V-shaped chromophores. For that, we applied the model described in detail in ref. 52 for sample in film form that describes the absorbance change over time due to the *trans* to *cis* photoisomerization. Such a model can be given by:

$$\frac{\mathrm{d}A(t)}{\mathrm{d}t} = -\frac{10^3\varphi\varepsilon I\left(1 - 10^{A(t)}\right)}{N_{\mathrm{A}}} \tag{4}$$

in which N_A is the Avogadro's number (mol^{-1}), ε is the molar absorptivity (which is 3.2×10^3 M^{-1} cm^{-1} at 532 nm), I is the fluence (photons per s per cm^2). Fig. 10(a) exhibits the absorbance change at 448 nm for different writing laser power.

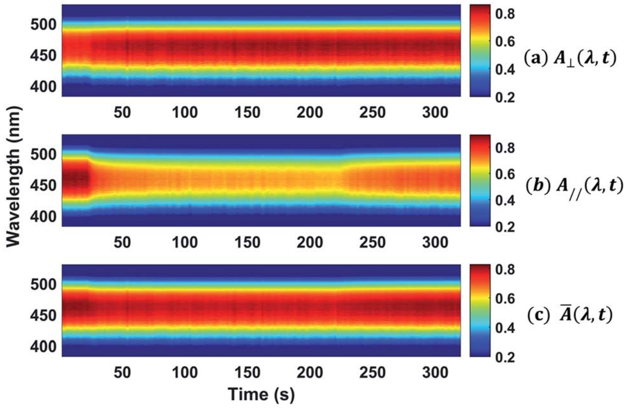

Fig. 8 Colormap representing the ground-state transient absorption for the (a) perpendicular and (b) parallel polarization and the (c) average absorption.

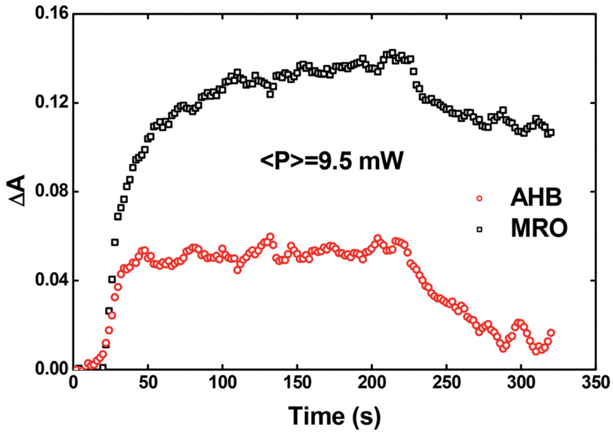

Fig. 9 AHB (circles) and MRO (squares) contributions to the optical birefringence.

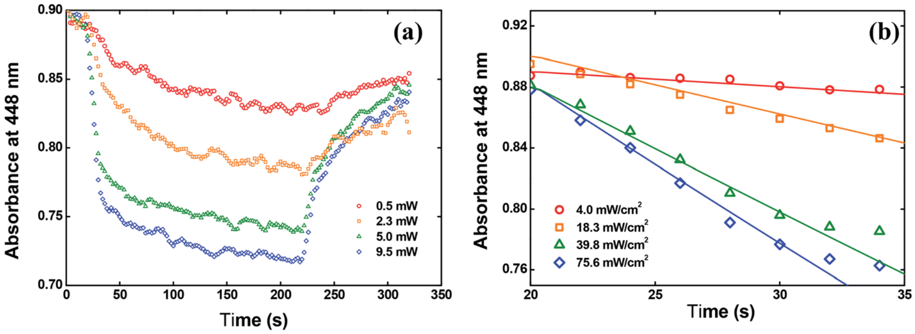

Fig. 10 (a) Absorbance change at 448 nm over time. (b) Fitting the data by using the eqn (4).

In Fig. 10(b), we showed the same results but only for the first 15 seconds after switching on the writing laser, because in this time interval the *trans* to *cis* isomerization occurs strongly. The solid lines in Fig. 10(b) are the fitting obtained by solving the eqn (4) numerically. From these fitting, we found $\varphi = 0.15 \pm 0.02$ at 532 nm for the solid-state sample. This value is almost twice the value reported for the red disperse family, for example.[29]

5. Final remarks

We have investigated the photoinduced birefringence in a V-shaped azo-chromophore/PMMA guest–host film. Our result pointed out a maximum optical birefringence of 3.3×10^{-4} along with the large residual optical memory (50%) in the low-concentration regime. The high performance for the optical birefringence observed in guest–host films can be explained as follows. The significant photoisomerization quantum yield (*trans–cis*) found for this material in solid-state (15%) is responsible for the high optical birefringence, which is preferentially related to the AHB mechanism. On the other hand, the large residual optical memory can be attributed to *cis–trans* MRO, in which our results have shown to be highly efficient (100%). Moreover, we have employed a simple model recently developed that corroborated these results, indicating that the MRO mechanism dominates the optical birefringence. Employing TD-DFT calculations, the contribution of the *cis*-isomers of the V-shaped azo-chromophore to the absorption spectrum of the guest–host film was confirmed. Moreover, potential energy curves (PECs) were constructed to investigate the possibility of the isomerization occur through thermal processes. Based on the values obtained for the energy barriers of the thermal *trans–cis* isomerization, $E_b = 3.42$ eV and $E_b = 4.02$ eV, for the mechanism of the rotation and inversion, respectively, we were led to conclude that the observed isomerization process is basically photoinduced. Finally, our outcomes indicate the V-shaped azo-chromophore as an interesting material for the development of photonic devices based on optical birefringence.

Conflicts of interest

There are no conflicts to declare.

Acknowledgements

Financial support from FAPEMIG (Fundação de Amparo à Pesquisa do Estado de Minas Gerais, APQ-01469-18), CNPq (Conselho Nacional de Desenvolvimento Científico e Tecnológico, 425180/2018-2), Coordenação de Aperfeiçoamento de Pessoal de Nível Superior (CAPES) are acknowledged.

References

1 S. Crespi, N. A. Simeth and B. Koinig, *Nat. Rev. Chem.*, 2019, **3**, 133–146.
2 R. Petruskevicius, D. Urbonas, M. Gabalis, A. Balcytis, G. Seniutinas, R. Tomasiunas, V. Getautis and IEEE, in *2013 15th International Conference on Transparent Optical Networks*, 2013.
3 P. Gopalan, H. E. Katz, D. J. McGee, C. Erben, T. Zielinski, D. Bousquet, D. Muller, J. Grazul and Y. Olsson, *J. Am. Chem. Soc.*, 2004, **126**, 1741–1747.
4 M. R. Cardoso, U. M. Neves, L. Misoguti, Z. H. Ye, X. R. Bu and C. R. Mendonca, *Opt. Mater.*, 2006, **28**, 1118–1122.
5 S. Hvilsted, C. Sanchez and R. Alcala, *J. Mater. Chem.*, 2009, **19**, 6641–6648.
6 A. H. Gelebart, D. J. Mulder, M. Varga, A. Konya, G. Vantomme, E. W. Meijer, R. L. B. Selinger and D. J. Broer, *Nature*, 2017, **546**, 632–636.
7 W. M. Gibbons, P. J. Shannon, S. T. Sun and B. J. Swetlin, *Nature*, 1991, **351**, 49–50.
8 C. Jones and S. Day, *Nature*, 1991, **351**, 15.
9 M. S. Ho, A. Natansohn and P. Rochon, *Macromolecules*, 1996, **29**, 44–49.
10 X. Meng, A. Natansohn and P. Rochon, *Polymer*, 1997, **38**, 2677–2682.
11 J. C. Liang, *Opt. Lett.*, 2010, **35**, 4081–4083.
12 D. S. dos Santos, A. Bassi, J. J. Rodrigues, L. Misoguti, O. N. Oliveira and C. R. Mendonca, *Biomacromolecules*, 2003, **4**, 1502–1505.
13 T. X. Gao, Y. J. Xue, Z. Zhang and W. X. Que, *Opt. Express*, 2018, **26**, 4309–4317.
14 M. Poprawa-Smoluch, J. Baggerman, H. Zhang, H. P. A. Maas, L. De Cola and A. M. Brouwer, *J. Phys. Chem. A*, 2006, **110**, 11926–11937.

15 T. Chida and Y. Kawabe, *Opt. Mater.*, 2014, **36**, 778–781.
16 L. Mazaheri, R. G. Sabat, O. Lebel and J. M. Nunzi, *Opt. Mater.*, 2016, **62**, 378–391.
17 F. Pirani, A. Angelini, F. Frascella, R. Rizzo, S. Ricciardi and E. Descrovi, *Sci. Rep.*, 2016, **6**, 31702.
18 A. Kovach, J. H. He, P. J. G. Saris, D. Y. Chen and A. M. Armani, *AIP Adv.*, 2020, **10**, 045117.
19 M. Sailer, R. Fernandez, X. Y. Lu and C. J. Barrett, *Phys. Chem. Chem. Phys.*, 2013, **15**, 19985–19989.
20 J. T. Huang, S. Beckemper, S. Wu, J. Shen, Q. J. Zhang, K. Y. Wang and A. Gillner, *Phys. Chem. Chem. Phys.*, 2011, **13**, 16150–16158.
21 B. Kulyk, D. Guichaoua, A. Ayadi, A. El-Ghayoury and B. Sahraoui, *Dyes Pigm.*, 2017, **145**, 256–262.
22 L. De Boni, L. Misoguti, S. C. Zilio and C. R. Mendonca, *ChemPhysChem*, 2005, **6**, 1121–1125.
23 U. M. Neves, L. De Boni, Z. H. Ye, X. R. Bu and C. R. Mendonca, *Chem. Phys. Lett.*, 2007, **441**, 221–225.
24 B. Jedrzejewska, M. Gordel, J. Szeremeta, M. A. Kaczorowska, M. Jozefowicz and M. Samoc, *Dyes Pigm.*, 2016, **132**, 237–247.
25 P. A. Blanche, P. C. Lemaire, M. Dumont and M. Fischer, *Opt. Lett.*, 1999, **24**, 1349–1351.
26 A. R. M. Timoteo, J. H. F. Ribeiro, P. A. Ribeiro and M. Raposo, *Opt. Mater.*, 2016, **51**, 18–23.
27 A. Stoilova, A. Georgiev, L. Nedelchev, D. Nazarova and D. Dimov, *Opt. Mater.*, 2019, **87**, 16–23.
28 C. R. Mendonca, U. M. Neves, L. De Boni, A. A. Andrade, D. S. dos Santos, F. J. Pavinatto, S. C. Zilio, L. Misoguti and O. N. Oliveira, *Opt. Commun.*, 2007, **273**, 435–440.
29 Y. Kawabe and K. Okoshi, *Opt. Mater. Express*, 2018, **8**, 332–341.
30 A. Goulet-Hanssens, T. C. Corkery, A. Priimagi and C. J. Barrett, *J. Mater. Chem. C*, 2014, **2**, 7505–7512.
31 D. M. Junge and D. V. McGrath, *J. Am. Chem. Soc.*, 1999, **121**, 4912–4913.
32 M. G. Vivas, D. L. Silva, L. De Boni, Y. Bretonniere, C. Andraud, F. Laibe-Darbour, J. C. Mulatier, R. Zalesny, W. Bartkowiak, S. Canuto and C. R. Mendonca, *J. Phys. Chem. B*, 2012, **116**, 14677–14688.
33 R. D. Fonseca, M. G. Vivas, D. L. Silva, G. Eucat, Y. Bretonniere, C. Andraud, L. De Boni and C. R. Mendonca, *J. Phys. Chem. C*, 2018, **122**, 1770–1778.
34 R. D. Fonseca, M. G. Vivas, D. L. Silva, G. Eucat, Y. Bretonniere, C. Andraud, C. R. Mendonca and L. De Boni, *J. Phys. Chem. Lett.*, 2019, **10**, 2214–2219.
35 R. Bakke and P. Q. Olsson, *J. Microbiol. Methods*, 1986, **5**, 93–98.
36 M. J. Frisch, H. B. Schlegel, G. E. Scuseria, M. A. Robb, G. Cheeseman, J. R. Scalmani, V. Barone, B. Mennucci, G. A. Petersson, H. Nakatsuji, M. Caricato, X. Li, H. P. Hratchian, A. F. Izmaylov, J. Bloino, G. Zheng, J. L. Sonnenberg, M. Hada, M. Ehara, K. Toyota, R. Fukuda, J. Hasegawa, M. Ishida, T. Nakajima, Y. Honda, O. Kitao, H. Nakai, T. Vreven, J. A. Montgomery, J. E. Peralta, F. Ogliaro, M. Bearpark, J. J. Heyd, E. Brothers, K. N. Kudin, R. Staroverov, V. N. Kobayashi, K. Normand, J. Raghavachari, A. Rendell, J. C. Burant, S. S. Iyengar, J. Tomasi, M. Cossi, N. Rega, N. J. Millam, M. Klene, J. E. Knox, J. B. Cross, V. Bakken, C. Adamo, J. Jaramillo, R. Gomperts, R. E. Stratmann, O. Yazyev, A. J. Austin, R. Cammi, C. Pomelli, J. W. Ochterski, R. L. Martin, K. Morokuma, V. G. Zakrzewski, G. A. Voth, P. Salvador, S. Dannenberg, J. J. Dapprich, A. D. Daniels, Ȯ. Farkas, J. B. Foresman, J. V. Ortiz, J. Cioslowski and D. J. Fox, *Gaussian 09, Revision D.01*, Gaussian, Inc., Wallingford, CT, 2013.
37 W. K. P. Hohenberg, *Phys. Rev.*, 1964, **136**, B864–B871.
38 W. Kohn and L. J. Sham, *Phys. Rev.*, 1965, **140**, 1133–1138.
39 A. D. Becke, *J. Chem. Phys.*, 1993, **98**, 5648–5652.
40 C. T. Lee, W. T. Yang and R. G. Parr, *Phys. Rev. B: Condens. Matter Mater. Phys.*, 1988, **37**, 785–789.
41 J. Tomasi, B. Mennucci and E. Cances, *J. Mol. Struct.: THEOCHEM*, 1999, **464**, 211–226.
42 E. Runge and E. K. U. Gross, *Phys. Rev. Lett.*, 1984, **52**, 997–1000.
43 M. S. Ho, A. Natansohn and P. Rochon, *Macromolecules*, 1995, **28**, 6124–6127.
44 C. H. Wang and R. G. Weiss, *Macromolecules*, 2003, **36**, 3833–3840.
45 M. Ueda, H. B. Kim, T. Ikeda and K. Ichimura, *Chem. Mater.*, 1992, **4**, 1229–1233.
46 S. Shinkai, Y. Kusano, K. Shigematsu and O. Manabe, *Chem. Lett.*, 1980, 1303–1306.
47 I. G. Marino, D. Bersani and P. P. Lottici, *Opt. Mater.*, 2000, **15**, 175–180.
48 A. Natansohn, P. Rochon, C. Barrett and A. Hay, *Chem. Mater.*, 1995, **7**, 1612–1615.
49 Y. Shuto, M. Amano and T. Kaino, *Electro-optical light modulation in novel azo-dye-substituted poled polymers*, 1991.
50 S. Elhani, I. Maouli, S. Refki, M. Halim, S. Hayashi and Z. Sekkat, *J. Opt.*, 2019, **21**, 115401.
51 S. Janssens, R. Breukers, A. Swanson and S. Raymond, *J. Appl. Phys.*, 2017, **122**, 023107.
52 K. Stranius and K. Borjesson, *Sci. Rep.*, 2017, **7**, 41145.